Energy Crisis in Human and Mouse Models of *SLC4A11*-associated Corneal Endothelial Dystrophies

Running Title: Energy Crisis in SLC4A11-deficient Corneal Endothelium

Wenlin Zhang[1], Ricardo Frausto[1], Doug Chung[1], Christopher G. Griffis[1], Liyo Kao[2], Angela Chen[1], Rustam Azimov[2], Alapakkam Sampath[1], Ira Kurtz[2, 3], Anthony Aldave[1]*

[1]Stein Eye Institute, UCLA, Los Angeles, CA 90095

[2]Division of Nephrology, David Geffen School of Medicine at UCLA, Los Angeles, CA 90095

[3]Brain Research Institute, UCLA, Los Angeles, CA 90095

*Corresponding Author: Anthony Aldave, aldave@jsei.ucla.edu

Conflict of Interests: There is no conflict of interests.

Abstract

Mutations in the solute-linked carrier family 4 member 11 (*SLC4A11)* gene are associated with congenital hereditary endothelial dystrophy (CHED), Fuchs endothelial corneal dystrophy and Harboyan syndrome, in all of which visually significant cornea edema may require corneal transplantation. However, the pathogenesis of SLC4A11-associated corneal endothelial dystrophies remains to be elucidated. Recent evidence suggested cellular respiration reprogramming and mitochondrial oxidative stress in SLC4A11-deficient corneal endothelium. Given the complexity of cellular metabolic regulation and its cell type specific impact on cellular physiology, we systemically analyzed the transcriptome of *SLC4A11* knock-down primary human corneal endothelium (*SLC4A11* KD pHCEnC) and corneal endothelial cells derived from *Slc4a11*$^{-/-}$ mice (*Slc4a11*$^{-/-}$ MCEnC) to provide a comprehensive characterization of the transcriptome profile changes resulting from loss of SLC4A11. To identify the conserved molecular mechanisms that lead to cornea endothelial dysfunction in both the human and murine models, we performed comparative transcriptomic analysis. Our analysis identified inhibition of cell metabolism and ion transport function as well as mitochondria dysfunction as shared between *SLC4A11* KD pHCEnC and *Slc4a11*$^{-/-}$ MCEnC. Functional analysis confirmed the absence of SLC4A11-mediated NH_4Cl-induced membrane depolarization in *Slc4a11*$^{-/-}$ MCEnC. Transcriptome of *SLC4A11* KD pHCEnC and *Slc4a11*$^{-/-}$ MCEnC identified downregulation of Na^+-HCO_3^- transporter (NBCe1, *SLC4A4*), a key player in corneal endothelial ‘pump’ function, and upregulation of Syntaxin 17 (*STX17*), an initiator of mitophagy. NBCe1 and STX17 were further analyzed in *Slc4a11*$^{-/-}$ MCEnC for functional impact and in *SLC4A11* KD pHCEnC and corneal endothelium from individuals with CHED for protein expression, all

showed consistent changes with transcriptome. CHED corneal endothelium also showed decreased immunostaining intensity for mitochondria markers suggesting decreased mitochondira density . In *SLC4A11* KD pHCEnC and *Slc4a11*$^{-/-}$ MCEnC, steady state ATP depletion and ATP sensing AMPK-p53 pathway activation were observed, consistent with the prediction using transcriptome data that transcriptional factor p53 were responsible for the transcriptomic changes. These findings suggest that insufficient energy fueling the corneal endothelial 'pump', as a result of metabolic inhibition and failing mitochondria, is the direct cause of clinical phenotype of corneal edema in *SLC4A11*-associated corneal endothelial dystrophies.

Key Words:

Congenital Hereditary Endothelial Dystrophy

Fuchs Endothelial Corneal Dystrophy

Harboyan Syndrome

SLC4A11

AMPK

P53

Mitochondria dysfunction

INTRODUCTION

Solute-linked carrier family 4 member 11 (SLC4A11) is one of the highly expressed differentiation markers for corneal endothelium [1-3]. Mutations in *SLC4A11* are associated with congenital hereditary endothelial dystrophy (CHED), Harboyan syndrome (CHED with perceptive deafness) and Fuchs endothelial corneal dystrophy (FECD) [4-7]. Additional evidence of a role for *SLC4A11* in FECD comes from reports of the hypermethylation of the *SLC4A11* promoter and transcriptional downregulation of *SLC4A11* in FECD corneal endothelium [8,9]. Children with CHED often present with bilateral corneal edema at or shortly after birth with significant vision impairment. Corneal transplantation is the only means of restoring vision and is associated with a guarded prognosis in terms of long term recovery of vision and graft survival [10]. In addition, these children are at risk of developing perceptive deafness later in life (Harboyan Syndrome) [11]. FECD affects as much as 5% of the U.S. population over 40 years of age [12], and visually significant corneal edema secondary to FECD is the most common indication for keratoplasty in US and worldwide [13,14]. Together, CHED and FECD constitute common indications for corneal transplantation in published series from around the world [15,16].

SLC4A11 is functionally characterized as an NH_3 and alkaline pH stimulated H^+ transporter, while permeability to Na^+, OH^- and water has also been reported [17-21]. SLC4A11 is essential in facilitating energy producing glutaminolysis, maintaining antioxidant signaling and preventing apoptosis in corneal endothelial cell [22-25]. During development and in the event of oxidative DNA damage, SLC4A11 gene expression is directly upregulated by activated p53 during development and in the response to DNA damage [26,27]. In SLC4A11-associated corneal endothelial

dystrophies, the cornea edema that develops as a result of pathologic *SLC4A11* mutations is evidence of corneal endothelial dysfunction, either from direct cell loss/death or from disturbances in the corneal endothelial 'pump-leak' system [28-30]. Corneal endothelial 'pump-leak' system achieves corneal transparency by maintaining the dynamic balance between the passive fluid leak from anterior chamber into corneal stroma and the active pump moving fluid from corneal stroma to anterior chamber. The fluid leak in corneal endothelium is particularly significant because hydrophilic glycosaminoglycans in the stroma are only 13~23% hydrated in physiological condition, producing a significant swelling pressure [31-33]. In addition, corneal endothelial tight junctions are focally incomplete, leading to a nonhomogeneous seal of the lateral intercellular space and offering little resistance to the paracellular passage of water and solutes [34-36]. The fluid pump activity is associated with a host of ion channels/exchangers/pumps positioned strategically at the apical and basolateral membranes of the corneal endothelial cells [29,37] and driven by an ionic electrical-chemical gradient set up by the highly expressed Na^+/K^+-ATPase [38]. As such, corneal endothelium has the second highest density of mitochondria among any cell types in the body (second to photoreceptors) to generate sufficient ATP to fuel the Na^+/K^+-ATPase driven endothelial 'pump'. As mentioned above, SLC4A11 plays a significant role in facilitating ATP-generating glutaminolysis in corneal endothelium [24]. Thus, it is not surprising that glutaminolysis inhibition, mitochondria membrane potential (MMP) depolarization, enriched mitochondrial reactive oxidative species (ROS) and increased mitochondria turnover have been observed in the corneal endothelium of the *Slc4a11*$^{-/-}$ mouse [24,25,39], which recapitulates the CHED corneal phenotype of significant cornea edema, Descemet membrane thickening and progressive corneal endothelial cell

loss [40]. Thus, the association between SLC4A11 and corneal endothelial mitochondrial function suggests SLC4A11 is involved not only in moving ions across the plasma membrane but also in the supply of energy to the endothelial 'pump'.

Approximately 94 mutations, including nonsense, missense, frameshift and intronic mutations, have been identified in *SLC4A11* in individuals with CHED [4,6,11,41-58]. Coding region mutations have been identified in 17 of the 19 exons of *SLC4A11*, with no spatial clustering within ~~to any of the xx functional domains of~~ SLC4A11 protein. While a large number of these mutations result in SLC4A11 protein misfolding and failure to mature to the plasma membrane [5,6,59-61], some mutations affect SLC4A11 transporter function without impacting membrane trafficking [19,62,63] or cause aberrant *SLC4A11* pre-mRNA splicing and subsequent reduced SLC4A11 expression [57]. Collectively, these observations suggest that loss of SLC4A11 function is the primary pathogenetic mechanism in CHED rather than mutant SLC4A11 protein misfolding/mislocalization in ER and secondary unfolded protein response. Therefore we investigated the impact of SLC4A11 reduction on the corneal endothelial transcriptome in human and murine corneal endothelial cells, with validation in corneal endothelium from individuals with CHED, and elucidated the upstream molecular mechanism leading to the observed transcriptomic changes.

MATERIALS AND METHODS

Isolation and Culturing of Primary Human Corneal Endothelial Cells

Primary cultures of human corneal endothelial cells (pHCEnC) were isolated from donor corneas as previously described [64]. Cells were plated in laminin coated cell culture plastic and cultured in a 1:1 mixture of F12-Ham's and M199 (F99) medium. Experiments were performed when the cells achieved an intact and confluent monolayer.

Knock-down of SLC4A11 in pHCEnC

Confluent pHCEnC were transfected with 10nM anti-SLC4A11 siRNA (siRNA-CrCrGrArArArGrUrArCrCrUrGrArArGrUrUrArArArGrArACT) or scrambled siRNA (OriGene Technologies) using Lipofectamine LTX (Life Technologies). At 72 hrs post-transfection, the cells were lysed in either Tri Reagent (Sigma-Aldrich) or radioimmunoprecipitation assay (RIPA) buffer for RNA and protein isolation, respectively.

Immortalized Mouse Corneal Endothelial Cell (MCEnC) Culture

Immortalized *Slc4a11*$^{+/+}$ and *Slc4a11*$^{-/-}$ MCEnC lines were derived from *Slc4a11*$^{+/+}$ and *Slc4a11*$^{-/-}$ mice corneal endothelium respectively as previously described [25]. All MCEnC lines were cultured on flasks coated with a mixture of 40 µg/cm^2 chondroitin sulfate (Sigma-Aldrich) and 40 ng/ cm^2 laminin (Sigma-Aldrich). Details of culture medium used can be found in supplemental material.

Total RNA Isolation from pHCEnC and MCEnC

Total RNA from cultured pHCEnC was isolated in TRI Reagent and purified with the RNeasy Clean-Up Kit (Qiagen). Total RNA from cultured MCEnC was isolated and purified using the RNeasy Plus Mini Kit (Qiagen). The integrity of the purified RNA

was analyzed by the Agilent 2100 Electrophoresis Bioanalyzer System (Agilent Technologies).

RNA Sequencing (RNA-Seq) of total RNA from pHCEnC and MCEnC

Purified total RNA from pHCEnC was prepared for RNA-seq libraries using KAPA mRNA HyperPrep Kit. Libraries were sequenced on the Illumina Hi-Seq 4000 and paired-end 150-bp reads were generated. Purified total RNA from MCEnC was submitted to the UCLA Technology Center for Genomics & Bioinformatics for library preparation and sequencing. Single-end 50-bp reads were generated using the Illumina Hi-seq 3000. The generated FASTQ files and quantitative results are available from the GEO DataSets database (accession number XXXXX and XXXXX; NCBI).

RNA-sequencing Data Analyses

The FASTQ files containing the raw reads from the pHCEnC and MCEnC were aligned to the human (GRCh38/hg38) and mouse (GRCm38/mm10) genomes respectively using Hisat2. The raw counts of aligned reads were converted to counts per million (CPM) mapped reads with consideration of library size and normalized by the method of trimmed mean of M values (TMM). Then linear models for microarray analysis (LIMMA) coupled with variance modeling at the observation-level (VOOM) were used for differential gene expression analysis in R software. The following thresholds defined differential expression: CPM > 1, fold change (fc) > 1, and adjusted p-value < 0.05. Differential gene expression (DGE) lists were obtained from the following sample sets respectively: pHCEnC sample set: passage 1 of pHCEnC with siRNA targeting *SLC4A11* versus scrambled RNA control (*SLC4A11* KD pHCEnC and scRNA pHCEnC; n=3 each); MCEnC early sample set: early passages of *Slc4a11*$^{-/-}$ MCEnC versus wild-type control (p6 *Slc4a11*$^{-/-}$ and p7 *Slc4a11*$^{+/+}$

MCEnC; n=4 each); and MCEnC late sample set: late passages of *Slc4a11*$^{-/-}$ MCEnC versus wild-type control (p39 *Slc4a11*$^{-/-}$ and p40 *Slc4a11*$^{+/+}$ MCEnC; n=4 each).

Ingenuity Pathway Analysis

Ingenuity Pathway Analysis (IPA®, QIAGEN Bioinformatics) was used to perform comparative transcriptome analysis among three sample sets (pHCEnC, MCEnC early and MCEnC late), canonical/biological function pathway enrichment and upstream regulator prediction analyses on each sample set. In the comparative transcriptome analysis, canonical and biological function pathways with a predicted activation z-score in each of the three sample sets were sorted by the sign and value of the z-score to identify the most enriched pathways. Enriched canonical and biological function pathways without an assigned z-score and predicted upstream regulators were ranked by mean enrichment p-values among sample sets.

Quantitative PCR

Quantitative PCR was performed to validate the differential expression of selected genes from transcriptome DGE list on separate batches of RNA samples from *SLC4A11* KD pHCEnC and *Slc4a11*$^{-/-}$ MCEnC. Total RNA of 1 µg from each sample was reversed transcribed using SuperScript III First-Strand synthesis kit (Sigma). Quantitative PCR was performed on the LightCycler 480 System (Roche) using the KAPA SYBR FAST Universal Kit (Kapa Biosystems) with an annealing temperature of 60 °C. Primers used are listed in Supplemental Table 1. Relative gene expression was obtained by comparison to the housekeeping gene *PPIA/Ppia or ACTB/Actb* and was calculated by the comparative Ct ($2^{-\Delta Ct}$) method.

Immunofluorescence

Five-micrometer sections of paraffin-embedded corneas from healthy donors and individuals with CHED were de-paraffinized and re-hydrated in a graded ethanol series (100%, 95% and 70% and 50%) for 5 min and subject to antigen retrieval in 10 mM Na-citrate. After blocking with 2% bovine serum albumin (BSA) in PBS, sections were incubated overnight at 4 °C with primary antibodies (listed in Supplemental Table 1) in 2% BSA. Slides were then incubated with 1:200 Alexa Fluor® 488 F(ab')2-Goat anti-Rabbit IgG (Invitrogen) and 1:200 Alexa Fluor® 568 F(ab')2-Goat Anti-Mouse IgG (Invitrogen) with DAPI in PBS with 2% BSA for one hour. Sections were mounted with prolong anti-fade mounting reagent (Invitrogen) and imaged with Olympus FV-1000 inverted confocal fluorescence microscope. Florescence intensity of the images were quantified using FLUOVIEW 4.2 and ImageJ software.

Single Cell Patch-clamp Recording

Single cell recordings were made from MCEnC cultured on 25-mm glass coverslips to ~10–20% confluence to isolate single adhered cells. Membrane voltages were measured using whole-cell patch electrodes in current clamp mode (I_{hold} = 0) as previously described [65]. Ammonium evoked responses were sampled at 1kHz and digitally low-pass filtered at 50Hz using a 7-pole Butterworth filter. Data were reported as mean (95%CI). Details of data acquisition and statistical analysis can be found in supplemental material.

Intracellular pH Measurement

Intracellular pH (pH_i) measurements were performed by monitoring intracellular free H^+ concentration using pH-sensitive fluorescent dye BCECF-AM (2′7′-bis(carboxyethyl)-5(6)-carboxyfluorescein-acetoxymethyl ester, B1170; Thermo

Fisher Scientific) as described previously [21,22]. Details of experimental settings can be found in supplemental material.

Western Blotting

Whole-cell lysates from pHCEnC and MCEnC were prepared with RIPA buffer with proteinase and phosphatase inhibitors. Total protein was quantified by bicinchoninic acid (BCA) assay, separated and detected on Simple Western system Wes™ (ProteinSimple). Quantification and data analysis were performed in Compass for SW software (ProteinSimple). Antibodies used are listed in Supplemental Table 1.

Intracellular ATP Assay

MCEnC and pHCEnC were seeded on 1×10^5 /mL in 12- and 24-well plates, respectively, and cultured to sub-confluence. ATP was extracted by a boiling water method [66], and measured using a luciferin-luciferase based ATP assay kit (Molecular Probes) following the manufacturer's instructions.

Statistical Analysis

Statistical analysis was performed in GraphPad Prism 7.0 software, unless otherwise indicated, with appropriate statistical tests based on the data structure. Specific statistical tests used for each comparison are indicated in figure legends. Data are presented as mean ± SEM unless otherwise indicated. Statistical significance is denoted as follows in the figures: $p < 0.05$, *; $p < 0.01$, **; $p<0.001$, ***; $p<0.0001$, ****.

RESULTS

SLC4A11 Mutations Do Not Result in Decreased Mutant SLC4A11 Expression

Corneal specimens two individuals with CHED were examined with light microscopy and immunocytochemistry. One of the two individuals (*SLC4A11*$^{Mu/Mu}$) demonstrated compound heterozygous mutations in *SLC4A11* (NM_001174090.1) c.[473_480delGCTTCGCCinsC];[2623C>T], p.[(R158PfsX3)];[(Arg875*)] and the other (*SLC4A11*$^{Mu/WT}$) demonstrated a single heterozygous *SLC4A11* coding region mutation [c.2146C>G (p.Pro716Ala)]. Both corneal specimens demonstrated a significantly thickened Descemet's membrane and an attenuated corneal endothelial layer with cytoplasmic inclusions present in some cells (Fig. 1A). Immunofluorescence staining for SLC4A11 protein in the corneal endothelium was performed in conjunction with the use of an antibody against an endoplasmic reticulum marker, protein disulfide isomerase (PDI), to investigate whether *SLC4A11* mutations lead to disease via protein misfolding and retention in the endoplasmic reticulum (ER), as previously reported [5,6,60]. There was no difference in the corneal endothelial SLC4A11 protein staining intensity between the two specimens from the individuals with CHED and seven healthy controls. In addition, the staining localized to the cellular membrane and did not co-localize with PDI (Fig. 1B). Thus, in the corneal endothelium of these two individuals with CHED, mutant SLC4A11 expression is not reduced compared to wild type SLC4A11 expression in controls, and remains localized to the cellular membrane instead of being retained in the ER.

SLC4A11/Slc4a11 Reduction Induces Corneal Endothelial Transcriptome Changes

Next, we performed transcriptome analysis in pHCEnC and MCEnC with reduced SLC4A11/Slc4a11, mimicking the loss of SLC4A11 function in CHED corneal endothelium. Principle component analysis (PCA) was performed to ensure tight

clustering within biological triplicates, and to ensure that the number of dimensions considered are sufficient in explaining the variances between samples of different genotypes (Supplemental Figure 1). Based on the shared corneal endothelial phenotypes between human CHED and the *Slc4a11*$^{-/-}$ mouse, we compared the transcriptomes from *SLC4A11* KD pHCEnC and early and late passage MCEnC derived from *Slc4a11*$^{-/-}$ mice (denoted as pHCEnC, MCEnC early and MCEnC late sample set, respectively) [25]. A comparison of the genes identified from each sample set that were differentially expressed in comparison to appropriate controls revealed 3171 genes that were consensually differentially expressed across three sample sets (Fig.1C), of which 1041 genes were differentially expressed in the same direction (Fig.1D). Over a third of the 30 most highly differentially expressed genes (Fig.1E) have been previously demonstrated to play important functional roles in the cornea and/or have been associated with corneal diseases, including *SEMA3E* [1], *MST1R* [67], *RNF43* [68], SLC2A3 [69], *WNK4* [70], SLC4A4 [71], *CYGB* [72], *SLC9A7* [1,73], *ZNF469* [74-77], *BNC1* [78] and *TTC22* [79].

Loss of SLC4A11 Leads to Generalized Inhibition of Cellular Metabolism

Comparison of enriched canonical pathway from *Slc4a11* KD pHCEnC, *Slc4a11*$^{-/-}$ MCEnC early and *Slc4a11*$^{-/-}$ MCEnC late sample sets identified a shared generalized inhibition (defined by negative activation z-score) of multiple metabolic pathways that were interconnected via intermediate metabolites (Fig.2A, B). A generalized decrease in the expression of enzyme-encoding genes in these pathways was observed (Fig.2C-I), a finding that was confirmed for selected genes from each pathway using qPCR (Fig.2J).

Altered Expression of Channels and Transporters Impairs Transport Function of Corneal Endothelium

IPA biological function enrichment analysis identified “transport of molecule” as the top inhibited function (negative z-score) shared between the transcriptomes of the pHCEnC, MCEnC early and late samples sets (Fig. 3A). Since SLC4A11 is an electrogenic NH_3:H^+ co-transporter [17], we performed single cell recording of membrane potential of *Slc4a11*$^{+/+}$ and *Slc4a11*$^{-/-}$ MCEnC in response to extracellularly perfused 10 mM NH_4Cl . While exposure to NH_4Cl induced a +12.7 mV (95% CI +5 mV, +20 mV) depolarization in *Slc4a11*$^{+/+}$ MCEnC, likely due to the NH_3:H^+ permeability provided by Slc4a11, exposure to NH_4Cl induced a -9.50 mV (95% CI -19.3 mV, -0.5 mV) hyperpolarization in *Slc4a11*$^{-/-}$ MCEnC (Fig. 3B, C).

To further understand the nature of this depolarization to hyperpolarization shift resulting from loss of Slc4a11, we examined the list of 1041 genes differentially expressed in the same direction in pHCEnC, MCEnC early and MCEnC late sample sets to identify channels and transporters with a $\log_2$FC > 1 (Fig. 3D). Twelve genes encoding ion channels were identified (Fig. 3D) including: Cl^- channels (*CLCN3*, *CLCN2*, *ANO5*) and Ca^{2+} channels (*TRPC1*, *TRPV4*, *CACNB1*, *CACNB4*, *TRPV2*), which were both up- and down-regulated; and K^+ channels (*KCNAB2*, *KCNMA1*), which were exclusively down-regulated. Twenty six genes encoding transporters were identified (Fig. 3D), 12 of which were upregulated and 14 of which were down regulated. including: Na^+-HCO_3^- co-transporter (*SLC4A4*), Ca^{2+}-ATPase (*ATP2B1*), glucose transporter (*SLC2A1, SLC2A13, SLC2A3, SLC2A12, SLC15A2*), glutamine transporter(*SLC38A1*), Cl^-/HCO_3^- exchanger (*SLC4A3*), ATP-binding cassette (ABC) transporters (*ABCA8, ABCC4*), K^+-Cl^- cotransporter (*SLC12A7*), Na^+/H^+ exchanger regulator (*SLC9A3R2*), Na^+-HPO_3^- co-transporter (*SLC20A1*), lactate transporter (*SLC16A4*), Na^+-carnitine co-transporter (SLC22A4, *SLC22A18*), SO_4^{2-} transporter (*SLC26A2*). In particular, electrogenic Na^+-HCO_3^- co-transporter (NBCe1, *SLC4A4*),

which plays an essential role in the corneal endothelial 'pump' function [29], was down-regulated 4 fold in *SLC4A11* KD pHCEnC and > 100 fold in *Slc4a11*$^{-/-}$ MCEnC (early and late passage) in transcriptomes of three sample sets (Fig.3D). The downregulation of SLC4A4/Slc4a4 was verified by qPCR in *SLC4A11* KD pHCEnC and *Slc4a11*$^{-/-}$ MCEnC (Fig. 3E) and by Western blot in *SLC4A11* KD pHCEnC (Fig. 3F). Immunofluorescence staining for NBCe1 (SLC4A4) in the corneal endothelium of two individuals with CHED showed decreased expression of NBCe1 compared to control cornea endothelium (Fig. 3G, H).

Next, direct functional measurement of Na^+ dependent HCO_3^- transport in *Slc4a11*$^{-/-}$ MCEnC showed reduced Na^+-HCO_3^- co-transporter activity when compared to *Slc4a11*$^{+/+}$ MCEnC (Fig. 3I). In Fig.3I, intracellar pH (pH_i) was maintained at a low value when *Slc4a11*$^{-/-}$ and *Slc4a11*$^{+/+}$ MCEnC were perfused with Na^+-free bicarbonate containing ([HCO_3^-] 28.3 mM) solution. When switched to a Na^+ containing bicarbonate solution, pH_i increased as the Na^+-HCO_3^- cotransporter (NBCe1) started to move the weak base HCO_3^- inward using Na^+ inward transmembrane electrochemical gradient. We determined the initial slope of this pH_i rise (pH_i recovery) to serve as an indirect measure of Na^+-HCO_3^- cotransport activity, and observed reduced Na^+ dependent pH_i recovery in *Slc4a11*$^{-/-}$ MCEC than *Slc4A11*$^{+/+}$ MCEnC (Fig. 3I, J).

Mitochondria Dysfunction Leads to Reduced ATP Production

Dilated mitochondria is a characteristic electron microscopy finding in CHED corneal endothelium, suggestive of mitochondrial involvement in the pathogenesis [80]. We identified "Mitochondria Dysfunction" is shared between pHCEnC and MCEnC early and late sample sets as the top enriched IPA canonical pathway (ranked by p-value, Fig. 4A). Correspondingly, in the list of 1041 genes differentially expressed in the

same direction in pHCEnC, MCEnC early and MCEnC late sample sets, genes encoding proteins involved in the mitochondria electron transport chain, mediating mitochondrial ATP flux, import machinery and translation machinery showed a generalized decreased expression (Fig. 4B, C). The transcriptomes also suggested 'autophagy' was activated (Fig.3A) in *SLC4A11* KD pHCEnC and *Slc4a11*$^{-/-}$ MCEnC. Together with the indication of "mitochondria dysfunction", we specifically examined the differential expression of the *STX17*/*Stx17* gene, which encodes SNARE protein Syntaxin 17 (STX17) and is an mitophagy initiator facilitating the removal of dysfunctional mitochondria [81]. *STX17/Stx17* was upregulated in the *SLC4A11* KD pHCEnC and *Slc4a11*$^{-/-}$ MCEnC transcriptomes (Fig. 4D), a finding that was validated by qPCR in *SLC4A11* KD pHCEnC and *Slc4a11*$^{-/-}$ MCEnC (Fig. 4E), by Western blot in *SLC4A11* KD pHCEnC (Fig. 4F) as well as by immunofluorescence, which demonstrated increased STX17 expression in CHED corneal endothelium compared with control (Fig. 4G). As STX17 can only mediate mitophagy where mitochondria are present, we co-stained for mitochondrial marker COX4 in CHED corneal endothelium and control (Fig. 4G), which demonstrated significantly decreased COX4 indicating reduced mitochondria density in CHED corneal endothelium (Fig.4G). Quantification of the relative STX17 abundance in reference to mitochondria density (STX17/COX4 ratio) showed increased STX17 level in CHED corneal endothelium (Fig. 4H). Quantification of COX4 staining intensity showed significantly reduced COX4 signal in CHED corneal endothelium than in healthy controls (Fig4 I). Staining CHED endothelium with another mitochondria marker, cytochrome C, also showed consistently decreased staining intensity (Fig. 4J, K).

Given the evidence indicating mitochondrial dysfunction and reduced mitochondria density in the setting of reduced SLC4A11 expression, we

hypothesized that this would result in insufficient ATP energy supply to maintain the Na^+-K^+-ATPase driven corneal endothelial 'pump', and the cornea edema that characterizes CHED. Thus, we performed a direct measurement of the steady state ATP levels in *SLC4A11* KD pHCEnC and *Slc4a11*$^{-/-}$ MCEnC, which revealed reduced ATP concentrations compared to control scRNA pHCEnC and *Slc4a11*$^{+/+}$ MCEnC, respectively (Fig. 4L, M).

Transcriptomic Changes Associated with Loss of SLC4A11 Are Mediated by Activation of AMPK-p53 Pathway

To identify the upstream signaling pathway leading to the observed transcriptomic changes in *SLC4A11* KD pHCEnC and *Slc4a11*$^{-/-}$ MCEnC, we performed upstream regulator prediction in IPA, which identified P53 (encoded by *TP53* gene) as the top candidate transcription factor (Fig. 5A). Western blot analysis in *SLC4A11* KD pHCEnC demonstrated increased Ser15 phosphorylation of p53 and an increased phosphorylated p53 / total p53 ratio compared to scRNA pHCEnC control (Fig. 5B), indicative of activation of p53 transcriptional activity. Similarly, in *Slc4a11*$^{-/-}$ MCEnC, we observed increased Ser18 phosphorylation of p53 (corresponding to Ser15 of human p53) in *Slc4a11*$^{-/-}$ MCEnC late passage, although this was not observed in early passage (Fig.5C). However, there was increased total p53 level in both *Slc4a11*$^{-/-}$ MCEnC early and late passages (Fig.5C, D), indicative of transcriptional activation of p53.

To identify the kinase responsible for the Ser15 (Ser18 in mouse) phosphorylation and transcriptional activation of p53, we investigated the role of the cellular ATP sensor AMP-activated protein kinase (AMPK), given the observed ATP depletion in *SLC4A11* KD pHEnC and *Slc4a11*$^{-/-}$ MCEnC as well as the reported capacity of AMPK to mediate Ser15 (Ser18 in mouse) phosphorylation and

transcriptional activation of p53 [82-84]. In the setting of a decreased ATP-to-ADP (or ATP-to-AMP) ratio, AMPK catalytic α subunit will be phosphorylated at Thr172 whereas phosphorylation of regulatory β1 subunit at Ser182 is not dependent upon cellular ATP level [85]. In *SLC4A11* KD pHCEnC and *Slc4a11*$^{-/-}$ MCEnC, we observed an increased ratio of Thr172 phosphorylated AMPKα / total AMPKα, and no change in the ratio of Ser182 phosphorylated AMPKβ1 / total AMPKβ1 (Fig. 5C).

DISCUSSION

In this manuscript, we utilized human and mouse corneal endothelial cell lines with reduced expression of SLC4A11/Slc4a11 to investigate the cause of corneal endothelial dysfunction that characterizes each of the *SLC4A11*-associated corneal endothelial dystrophies (CHED, FECD and Harboyan syndrome. While several previous reports have elucidated possible roles for mitochondrial uncoupling, ER unfolded protein response, oxidative stress and apoptosis in SLC4A11-deficient cell lines [11,22,23,39,60,86], only one report examined CHED patient corneal endothelium and demonstrated increased oxidative stress [22]. We identified ATP depletion in corneal endothelial lacking SLC4A11/Slc4a11, in both transient (72 hours) *SLC4A11* knock-down pHCEnC and permanent *Slc4a11* knockout MCEnC through prolonged passage (early vs late passage). The reduced corneal endothelial ATP levels provide a proposed pathogenesis for the corneal endothelial dysfunction, which clinically manifested as corneal edema. The fact that ATP depletion and ATP-sensor AMPKα activation were detected within 72 hours of *SLC4A11* knock-down in pHCEnC suggests this energy shortage from the loss of SLC4A11 function is likely the initial step in the pathogenesis of *SLC4A11*-associated corneal endothelial dystrophies that leads to the downstream cascade of oxidative stress and apoptotic cell loss.

When examining the expression and localization of SLC4A11 protein in CHED corneal endothelium, we provide the initial evidence that mutant SLC4A11 protein is not retained in the ER of the corneal endothelium. While the prevailing hypothesis is that majority of *SLC4A11* mutations result in protein misfolding and retention in the endoplasmic reticulum [5,6,60,61], supporting evidence is from overexpression of SLC4A11 mutants in a HEK293 cell line model. Mutant SLC4A11 localization was

neither investigated in corneal endothelial cells overexpressing SLC4A11 mutants nor in corneal endothelium from individuals with CHED. In addition, our immunostaining of CHED corneal endothelium did not show reduced expression level of the SLC4A11 mutant protein, consistent with the previous report that CHED corneal endothelium does not demonstrate reduced SLC4A11 expression at the mRNA level [22]. Instead, our data supports the alternative hypothesis that identified *SLC4A11* mutations affect the protein transport function of the SLC4A11 protein in the corneal endothelium [19,62,63].

We used a comparative transcriptomics approach based on the observation of phenotypic similarities between CHED and the *Slc4a11*$^{-/-}$ mouse corneal phenotype [40,87]. This approach is based on the high degree of gene orthology between mouse and human and the organ-dominated hierarchical clustering observed across mammals on real genes expression data [88]. Comparative transcriptomic analysis of human and mouse sample sets together is advantageous over independent transcriptomic analysis of each sample set as it enables us to identify transcriptome determinants attributable to the loss of SLC4A11/Slc4a11 from that resulting from other biological factors or technical effects such as primary cell passage numbers, cell line immortalization, siRNA treatment, differences in culture medium and etc [89]. With this approach, we identified generalized inhibition of multiple metabolic pathways, as well as mitochondria dysfunction in both *SLC4A11* KD pHCEnC and *Slc4a11*$^{-/-}$ MCEnC, mediated via the activation of the AMPK-p53 pathway. The data presented here support the use of the *Slc4a11*$^{-/-}$ mice as a model for the *SLC4A11* associated corneal endothelial dystrophies and indicate a favorable translational potential for therapeutic approaches shown to be efficacious in the *Slc4a11*$^{-/-}$ mice.

When investigating the impact of reduced SLC4A11 on molecule transport function in corneal endothelial cells, we demonstrated opposite NH_4Cl induced membrane potential change in *Slc4a11*$^{-/-}$ versus *Slc4a11*$^{+/+}$ MCEnC. Membrane depolarization in reaction to extracellular NH_4Cl exposure were commonly observed in membranes with permeability to NH_4^+/NH_3 (membranes expressing ammonia or ammonium transporters/channels such as AQP8, AQP4, AMT1 and Rh-associated glycoproteins) [90,91]. In *Slc4a11*$^{+/+}$ MCEnC, extracellular NH_4Cl perfusion induced similar membrane depolarization. However, in *Slc4a11*$^{-/-}$ MCEnC, hyperpolarization was observed. Transcriptome data showed differential expression of 38 ion channels and transporters, suggesting SLC4A11 not only facilitates NH_4^+/NH_3 transmembrane movement but may also functions in maintaining the homeostasis of the endothelial transmembrane ion gradient by regulating the expression and function of other channels/transporters. This hypothesis is supported by the observation of reduced expression and activity of the Na^+-HCO_3^- co-transporter (NBCe1, *SLC4A4*) in *Slc4a11*$^{-/-}$ MCEnC. Future investigation analyzing the activity of other differentially expressed ion channels and transporters is needed to facilitate our detailed understanding of the impact of SLC4A11 reduction on corneal endothelial “pump function”.

Our attempt to identify upstream determinants of the observed transcriptomic changes revealed activation of AMPK-p53 pathway in *SLC4A11* KD pHCEnC and *Slc4a11*$^{-/-}$ MCEnC. Our data suggests that AMPK activation is likely to be the initial cellular event in response to SLC4A11 deficiency induced ATP depletion. While there was consistent AMPK activation (increased Thr172 phosphorylation) in both acute SLC4A11 deficiency in pHCEnC and chronic SLC4A11 deficiency in MCEnC, and increased p53 phosphorylation at Ser15 (or Ser18 in mouse) was only observed

in *SLC4A11* KD pHCEnC and *Slc4a11*$^{-/-}$ MCEnC late passage, but not in *Slc4a11*$^{-/-}$ MCEnC early passage. However, total p53 level was elevated in both early and late passages of MCEnC with permeant knockout of *Slc4a11*. Although p53 is generally stablely expressed at the protein level, recent evidence suggests activation of AMPKα can induce the transcriptional activation of *p53* [83]. In the context of our data, it suggests that short-term AMPKα activation in SLC4A11 deficiency induced post-translational activation of p53, whereas prolonged AMPKα activation in SLC4A11 deficiency induced transcriptional activation of p53.

ACKNOWLEDGEMENTS

We genuinely thank Dr. Huong Duong in Ho Chi Minh City Eye Hospital for facilitating the acquisition of postsurgical corneal endothelium specimens from individuals with CHED.

Support is provided by National Eye Institute Grants 1R01EY022082 (A.J.A.), P30EY000331 (core grant), the Walton Li Chair in Cornea and Uveitis (A.J.A.), the Stotter Revocable Trust (SEI Cornea Division), an unrestricted grant from Research to Prevent Blindness (A.J.A.), National Institute of Diabetes and Digestive and Kidney Diseases 1R01DK077162 (I.K.), the Allan Smidt Charitable Fund (I.K.), Ralph Block Family Foundation (I.K.) and Knights Templar Eye Foundation Career Starter Grant (WZ).

STATEMENT OF AUTHOR CONTRIBUTIONS

W.Z., R.F., C.G.G., L.K.and A.J.A. conceived the experiments, W.Z. and A.J.A. wrote the manuscript, W.Z., R.F., D.C, C.G.G., L.K., A.C. and R.A. performed the experiments. W.Z. A.S., I.K., and A.J.A. secured funding. A.S. and I.K. provided expertise and feedback.

REFERENCE LIST

1. Frausto RF, Wang C, Aldave AJ. Transcriptome Analysis of the Human Corneal Endothelium. *Investigative Ophthalmology & Visual Science* 2014; **55**: 7821-7830.
2. Chng Z, Peh GS, Herath WB*, et al.* High throughput gene expression analysis identifies reliable expression markers of human corneal endothelial cells. *PLoS One* 2013; **8**: e67546.
3. Chen Y, Huang K, Nakatsu MN*, et al.* Identification of novel molecular markers through transcriptomic analysis in human fetal and adult corneal endothelial cells. *Human Molecular Genetics* 2012; **22**: 1271-1279.
4. Aldahmesh MA, Khan AO, Meyer BF*, et al.* Mutational spectrum of SLC4A11 in autosomal recessive CHED in Saudi Arabia. *Invest Ophthalmol Vis Sci* 2009; **50**: 4142-4145.
5. Vithana EN, Morgan PE, Ramprasad V*, et al.* SLC4A11 mutations in Fuchs endothelial corneal dystrophy. *Hum Mol Genet* 2008; **17**: 656-666.
6. Vithana EN, Morgan P, Sundaresan P*, et al.* Mutations in sodium-borate cotransporter SLC4A11 cause recessive congenital hereditary endothelial dystrophy (CHED2). *Nat Genet* 2006; **38**: 755-757.
7. Desir J, Moya G, Reish O*, et al.* Borate transporter SLC4A11 mutations cause both Harboyan syndrome and non-syndromic corneal endothelial dystrophy. *J Med Genet* 2007; **44**: 322-326.
8. Khuc E, Bainer R, Wolf M*, et al.* Comprehensive characterization of DNA methylation changes in Fuchs endothelial corneal dystrophy. *PLoS One* 2017; **12**: e0175112.
9. Gottsch JD, Bowers AL, Margulies EH*, et al.* Serial Analysis of Gene Expression in the Corneal Endothelium of Fuchs' Dystrophy. *Investigative Ophthalmology & Visual Science* 2003; **44**: 594-599.
10. Dana M-R, Moyes AL, Gomes JAP*, et al.* The Indications for and Outcome in Pediatric Keratoplasty: A Multicenter Study. *Ophthalmology* 1995; **102**: 1129-1138.
11. Siddiqui S, Zenteno JC, Rice A*, et al.* Congenital hereditary endothelial dystrophy caused by SLC4A11 mutations progresses to Harboyan syndrome. *Cornea* 2014; **33**: 247-251.
12. Lorenzetti DW, Uotila MH, Parikh N*, et al.* Central cornea guttata. Incidence in the general population. *Am J Ophthalmol* 1967; **64**: 1155-1158.
13. 2018 Eye Banking Statistical Report. *Eye Bank Association of America* 2019.
14. Gain P, Jullienne R, He Z*, et al.* Global Survey of Corneal Transplantation and Eye Banking. *JAMA Ophthalmology* 2016; **134**: 167-173.
15. Dorrepaal SJ, Cao KY, Slomovic AR. Indications for penetrating keratoplasty in a tertiary referral centre in Canada, 1996-2004. *Can J Ophthalmol* 2007; **42**: 244-250.
16. Ghosheh FR, Cremona FA, Rapuano CJ*, et al.* Trends in penetrating keratoplasty in the United States 1980-2005. *Int Ophthalmol* 2008; **28**: 147-153.
17. Zhang W, Ogando DG, Bonanno JA*, et al.* Human SLC4A11 Is a Novel NH3/H+ Co-transporter. *J Biol Chem* 2015; **290**: 16894-16905.
18. Myers EJ, Marshall A, Jennings ML*, et al.* Mouse Slc4a11 expressed in Xenopus oocytes is an ideally selective H+/OH- conductance pathway that is stimulated by rises in intracellular and extracellular pH. *Am J Physiol Cell Physiol* 2016; **311**: C945-C959.
19. Vilas GL, Loganathan SK, Liu J*, et al.* Transmembrane water-flux through SLC4A11: a route defective in genetic corneal diseases. *Hum Mol Genet* 2013; **22**: 4579-4590.
20. Ogando DG, Jalimarada SS, Zhang W*, et al.* SLC4A11 is an EIPA-sensitive Na(+) permeable pHi regulator. *Am J Physiol Cell Physiol* 2013; **305**: C716-727.
21. Kao L, Azimov R, Shao XM*, et al.* Multifunctional ion transport properties of human SLC4A11: comparison of the SLC4A11-B and SLC4A11-C variants. *Am J Physiol Cell Physiol* 2016; **311**: C820-C830.

22. Guha S, Chaurasia S, Ramachandran C*, et al.* SLC4A11 depletion impairs NRF2 mediated antioxidant signaling and increases reactive oxygen species in human corneal endothelial cells during oxidative stress. *Sci Rep* 2017; **7**: 4074.
23. Liu J, Seet LF, Koh LW*, et al.* Depletion of SLC4A11 causes cell death by apoptosis in an immortalized human corneal endothelial cell line. *Invest Ophthalmol Vis Sci* 2012; **53**: 3270-3279.
24. Zhang W, Li H, Ogando DG*, et al.* Glutaminolysis is Essential for Energy Production and Ion Transport in Human Corneal Endothelium. *EBioMedicine* 2017; **16**: 292-301.
25. Zhang W, Ogando DG, Kim ET*, et al.* Conditionally Immortal Slc4a11-/- Mouse Corneal Endothelial Cell Line Recapitulates Disrupted Glutaminolysis Seen in Slc4a11-/- Mouse Model. *Invest Ophthalmol Vis Sci* 2017; **58**: 3723-3731.
26. Wang Q, Zou Y, Nowotschin S*, et al.* The p53 Family Coordinates Wnt and Nodal Inputs in Mesendodermal Differentiation of Embryonic Stem Cells. *Cell Stem Cell* 2017; **20**: 70-86.
27. Younger ST, Kenzelmann-Broz D, Jung H*, et al.* Integrative genomic analysis reveals widespread enhancer regulation by p53 in response to DNA damage. *Nucleic Acids Res* 2015; **43**: 4447-4462.
28. Edelhauser HF. The balance between corneal transparency and edema: the Proctor Lecture. *Invest Ophthalmol Vis Sci* 2006; **47**: 1754-1767.
29. Bonanno JA. Molecular mechanisms underlying the corneal endothelial pump. *Exp Eye Res* 2012; **95**: 2-7.
30. Srinivas SP. Dynamic regulation of barrier integrity of the corneal endothelium. *Optom Vis Sci* 2010; **87**: E239-254.
31. Hedblom EE. The role of polysaccharides in corneal swelling. *Exp Eye Res* 1961; **1**: 81-91.
32. Hedbys BO, Mishima S, Maurice DM. The Imbibition Pressure of the Corneal Stroma. *Exp Eye Res* 1963; **2**: 99-111.
33. Maurice DM. The transparency of the corneal stroma. *Vision research* 1970; **10**: 107-108.
34. Noske W, Fromm M, Levarlet B*, et al*. Tight junctions of the human corneal endothelium: morphological and electrophysiological features. *Ger J Ophthalmol* 1994; **3**: 253-257.
35. Ma L, Kuang K, Smith RW*, et al.* Modulation of tight junction properties relevant to fluid transport across rabbit corneal endothelium. *Exp Eye Res* 2007; **84**: 790-798.
36. Maurice DM, Srinivas SP. Fluorometric measurement of light absorption by the rabbit cornea. *Exp Eye Res* 1994; **58**: 409-413.
37. Bonanno JA. Identity and regulation of ion transport mechanisms in the corneal endothelium. *Prog Retin Eye Res* 2003; **22**: 69-94.
38. Riley MV, Winkler BS, Peters MI*, et al.* Relationship between fluid transport and in situ inhibition of Na(+)-K+ adenosine triphosphatase in corneal endothelium. *Invest Ophthalmol Vis Sci* 1994; **35**: 560-567.
39. Ogando DG, Choi M, Shyam R*, et al.* Ammonia sensitive SLC4A11 mitochondrial uncoupling reduces glutamine induced oxidative stress. *Redox Biology* 2019; **26**: 101260.
40. Han SB, Ang HP, Poh R*, et al.* Mice with a targeted disruption of Slc4a11 model the progressive corneal changes of congenital hereditary endothelial dystrophy. *Invest Ophthalmol Vis Sci* 2013; **54**: 6179-6189.
41. Jiao X, Sultana A, Garg P*, et al.* Autosomal recessive corneal endothelial dystrophy (CHED2) is associated with mutations in SLC4A11. *J Med Genet* 2007; **44**: 64-68.
42. Hemadevi B, Veitia RA, Srinivasan M*, et al.* Identification of mutations in the SLC4A11 gene in patients with recessive congenital hereditary endothelial dystrophy. *Archives of ophthalmology* 2008; **126**: 700-708.
43. Sultana A, Garg P, Ramamurthy B*, et al.* Mutational spectrum of the SLC4A11 gene in autosomal recessive congenital hereditary endothelial dystrophy. *Mol Vis* 2007; **13**: 1327-1332.

44. Aldave AJ, Yellore VS, Bourla N, *et al.* Autosomal recessive CHED associated with novel compound heterozygous mutations in SLC4A11. *Cornea* 2007; **26**: 896-900.
45. Ramprasad VL, Ebenezer ND, Aung T, *et al.* Novel SLC4A11 mutations in patients with recessive congenital hereditary endothelial dystrophy (CHED2). Mutation in brief #958. Online. *Human mutation* 2007; **28**: 522-523.
46. Shah SS, Al-Rajhi A, Brandt JD, *et al.* Mutation in the SLC4A11 gene associated with autosomal recessive congenital hereditary endothelial dystrophy in a large Saudi family. *Ophthalmic Genet* 2008; **29**: 41-45.
47. Kumar A, Bhattacharjee S, Prakash DR, *et al.* Genetic analysis of two Indian families affected with congenital hereditary endothelial dystrophy: two novel mutations in SLC4A11. *Mol Vis* 2007; **13**: 39-46.
48. Paliwal P, Sharma A, Tandon R, *et al.* Congenital hereditary endothelial dystrophy - mutation analysis of SLC4A11 and genotype-phenotype correlation in a North Indian patient cohort. *Mol Vis* 2010; **16**: 2955-2963.
49. Liskova P, Dudakova L, Tesar V, *et al.* Detailed assessment of renal function in a proband with Harboyan syndrome caused by a novel homozygous SLC4A11 nonsense mutation. *Ophthalmic research* 2015; **53**: 30-35.
50. Kodaganur SG, Kapoor S, Veerappa AM, *et al.* Mutation analysis of the SLC4A11 gene in Indian families with congenital hereditary endothelial dystrophy 2 and a review of the literature. *Mol Vis* 2013; **19**: 1694-1706.
51. Park SH, Jeong HJ, Kim M, *et al.* A novel nonsense mutation of the SLC4A11 gene in a Korean patient with autosomal recessive congenital hereditary endothelial dystrophy. *Cornea* 2013; **32**: e181-182.
52. Kumawat BL, Gupta R, Sharma A, *et al.* Delayed onset of congenital hereditary endothelial dystrophy due to compound heterozygous SLC4A11 mutations. *Indian J Ophthalmol* 2016; **64**: 492-495.
53. Kim JH, Ko JM, Tchah H. Fuchs Endothelial Corneal Dystrophy in a Heterozygous Carrier of Congenital Hereditary Endothelial Dystrophy Type 2 with a Novel Mutation in SLC4A11. *Ophthalmic Genet* 2015; **36**: 284-286.
54. Kaul H, Suman M, Khan Z, *et al.* Missense mutation in SLC4A11 in two Pakistani families affected with congenital hereditary endothelial dystrophy (CHED2). *Clin Exp Optom* 2016; **99**: 73-77.
55. Cunnusamy K, Bowman CB, Beebe W, *et al.* Congenital Corneal Endothelial Dystrophies Resulting From Novel De Novo Mutations. *Cornea* 2016; **35**: 281-285.
56. Hand CK, McGuire M, Parfrey NA, *et al.* Homozygous SLC4A11 mutation in a large Irish CHED2 pedigree. *Ophthalmic Genet* 2017; **38**: 148-151.
57. Brejchova K, Dudakova L, Skalicka P, *et al.* IPSC-Derived Corneal Endothelial-like Cells Act as an Appropriate Model System to Assess the Impact of SLC4A11 Variants on Pre-mRNA SplicingCorneal Endothelial-like Cells Expressing SLC4A11. *Investigative Ophthalmology & Visual Science* 2019; **60**: 3084-3090.
58. Moazzeni H, Javadi MA, Asgari D, *et al.* Observation of nine previously reported and 10 non-reported SLC4A11 mutations among 20 Iranian CHED probands and identification of an MPDZ mutation as possible cause of CHED and FECD in one family. *British Journal of Ophthalmology* 2019: e314377.
59. Alka K, Casey JR. Ophthalmic Nonsteroidal Anti-Inflammatory Drugs as a Therapy for Corneal Dystrophies Caused by SLC4A11 Mutation. *Invest Ophthalmol Vis Sci* 2018; **59**: 4258-4267.
60. Alka K, Casey JR. Molecular phenotype of SLC4A11 missense mutants: Setting the stage for personalized medicine in corneal dystrophies. *Human mutation* 2018; **39**: 676-690.
61. Malhotra D, Loganathan SK, Chiu AM, *et al.* Human Corneal Expression of SLC4A11, a Gene Mutated in Endothelial Corneal Dystrophies. *Scientific Reports* 2019; **9**: 9681.

62. Li S, Hundal KS, Chen X, *et al.* R125H, W240S, C386R, and V507I SLC4A11 mutations associated with corneal endothelial dystrophy affect the transporter function but not trafficking in PS120 cells. *Exp Eye Res* 2019; **180**: 86-91.
63. Kao L, Azimov R, Abuladze N, *et al.* Human SLC4A11-C functions as a DIDS-stimulatable H(+)(OH(-)) permeation pathway: partial correction of R109H mutant transport. *Am J Physiol Cell Physiol* 2015; **308**: C176-188.
64. Frausto RF, Le DJ, Aldave AJ. Transcriptomic Analysis of Cultured Corneal Endothelial Cells as a Validation for Their Use in Cell Replacement Therapy. *Cell Transplant* 2016; **25**: 1159-1176.
65. Wang T, Pahlberg J, Cafaro J, *et al.* Activation of Rod Input in a Model of Retinal Degeneration Reverses Retinal Remodeling and Induces Formation of Functional Synapses and Recovery of Visual Signaling in the Adult Retina. *J Neurosci* 2019; **39**: 6798-6810.
66. Yang NC, Ho WM, Chen YH, *et al.* A convenient one-step extraction of cellular ATP using boiling water for the luciferin-luciferase assay of ATP. *Anal Biochem* 2002; **306**: 323-327.
67. Swamynathan SK, Davis J, Piatigorsky J. Identification of candidate Klf4 target genes reveals the molecular basis of the diverse regulatory roles of Klf4 in the mouse cornea. *Invest Ophthalmol Vis Sci* 2008; **49**: 3360-3370.
68. Okumura N, Nakamura T, Kay EP, *et al.* R-spondin1 regulates cell proliferation of corneal endothelial cells via the Wnt3a/beta-catenin pathway. *Invest Ophthalmol Vis Sci* 2014; **55**: 6861-6869.
69. Chng Z, Peh GSL, Herath WB, *et al.* High Throughput Gene Expression Analysis Identifies Reliable Expression Markers of Human Corneal Endothelial Cells. *PLoS ONE* 2013; **8**: e67546.
70. Shimizu M, Goto T, Sato A, *et al.* WNK4 is an essential effector of anterior formation in FGF signaling. *Genes Cells* 2013; **18**: 442-449.
71. Bonanno JA. Molecular mechanisms underlying the corneal endothelial pump. *Experimental eye research* 2012; **95**: 2-7.
72. Ostojic J, Grozdanic S, Syed NA, *et al.* Neuroglobin and cytoglobin distribution in the anterior eye segment: a comparative immunohistochemical study. *J Histochem Cytochem* 2008; **56**: 863-872.
73. Cheong YK, Ngoh ZX, Peh GS, *et al.* Identification of cell surface markers glypican-4 and CD200 that differentiate human corneal endothelium from stromal fibroblasts. *Invest Ophthalmol Vis Sci* 2013; **54**: 4538-4547.
74. Yildiz E, Bardak H, Gunay M, *et al.* Novel Zinc Finger Protein Gene 469 (ZNF469) Variants in Advanced Keratoconus. *Curr Eye Res* 2017; **42**: 1396-1400.
75. Vincent AL, Jordan CA, Cadzow MJ, *et al.* Mutations in the zinc finger protein gene, ZNF469, contribute to the pathogenesis of keratoconus. *Invest Ophthalmol Vis Sci* 2014; **55**: 5629-5635.
76. Lechner J, Porter LF, Rice A, *et al.* Enrichment of pathogenic alleles in the brittle cornea gene, ZNF469, in keratoconus. *Hum Mol Genet* 2014; **23**: 5527-5535.
77. Lu Y, Dimasi DP, Hysi PG, *et al.* Common genetic variants near the Brittle Cornea Syndrome locus ZNF469 influence the blinding disease risk factor central corneal thickness. *PLoS Genet* 2010; **6**: e1000947.
78. Zhang X, Tseng H. Basonuclin-null mutation impairs homeostasis and wound repair in mouse corneal epithelium. *PLoS One* 2007; **2**: e1087.
79. Chung DD, Frausto RF, Lin BR, *et al.* Transcriptomic Profiling of Posterior Polymorphous Corneal Dystrophy. *Invest Ophthalmol Vis Sci* 2017; **58**: 3202-3214.
80. Ehlers N, Modis L, Moller-Pedersen T. A morphological and functional study of Congenital Hereditary Endothelial Dystrophy. *Acta Ophthalmol Scand* 1998; **76**: 314-318.
81. Xian H, Yang Q, Xiao L, *et al.* STX17 dynamically regulated by Fis1 induces mitophagy via hierarchical macroautophagic mechanism. *Nature Communications* 2019; **10**: 2059.

82. Nieminen AI, Eskelinen VM, Haikala HM*, et al.* Myc-induced AMPK-phospho p53 pathway activates Bak to sensitize mitochondrial apoptosis. *Proceedings of the National Academy of Sciences* 2013; **110**: E1839-E1848.
83. Okoshi R, Ozaki T, Yamamoto H*, et al.* Activation of AMP-activated Protein Kinase Induces p53-dependent Apoptotic Cell Death in Response to Energetic Stress. *Journal of Biological Chemistry* 2008; **283**: 3979-3987.
84. Jones RG, Plas DR, Kubek S*, et al.* AMP-Activated Protein Kinase Induces a p53-Dependent Metabolic Checkpoint. *Molecular Cell* 2005; **18**: 283-293.
85. Herzig S, Shaw RJ. AMPK: guardian of metabolism and mitochondrial homeostasis. *Nature Reviews Molecular Cell Biology* 2017; **19**: 121.
86. Loganathan SK, Casey JR. Corneal dystrophy-causing SLC4A11 mutants: suitability for folding-correction therapy. *Human mutation* 2014; **35**: 1082-1091.
87. Kirkness CM, McCartney A, Rice NS*, et al.* Congenital hereditary corneal oedema of Maumenee: its clinical features, management, and pathology. *Br J Ophthalmol* 1987; **71**: 130-144.
88. Breschi A, Djebali S, Gillis J*, et al.* Gene-specific patterns of expression variation across organs and species. *Genome Biology* 2016; **17**: 151.
89. Breschi A, Gingeras TR, Guigo R. Comparative transcriptomics in human and mouse. *Nat Rev Genet* 2017; **18**: 425-440.
90. Assentoft M, Kaptan S, Schneider H-P*, et al.* Aquaporin 4 as a NH3 Channel. *The Journal of biological chemistry* 2016; **291**: 19184-19195.
91. Mak D-OD, Dang B, Weiner ID*, et al.* Characterization of ammonia transport by the kidney Rh glycoproteins RhBG and RhCG. *American Journal of Physiology-Renal Physiology* 2006; **290**: F297-F305.

FIGURE LEGEND

Figure 1. SLC4A11 deficiency leads to transcriptome alteration in corneal endothelium. (A) Histopathologic examination of control and CHED corneas demonstrating Descemet membrane thickening and endothelial cell attenuation in corneas from individuals with CHED (H&E stain, scale bar, 25 µm). (B) Left: representative images of immunofluorescence staining for SLC4A11 (green signal) and ER marker PDI (red signal) in corneal endothelium of two individuals with CHED and healthy control. Nucleus were stained with DAPI (blue signal) (Scale bar, 100 µm); Right: scatterplot of mean fluorescence intensity (MFI) ratio of SLC4A11 over PDI in corneal endothelium of two individuals with CHED and of 7 healthy controls. (two-tailed unpaired t-test with Welch's correction, $p = 0.5127$). (C) Venn diagram of the endothelial transcriptome in *SLC4A11* KD pHCEnC, *Slc4a11*$^{-/-}$ MCEnC early and late passages indicating the number of differentially expressed genes (DEG) in each of the sample sets. (D) Venn diagram of the endothelial transcriptome in *SLC4A11* KD pHCEnC, *Slc4a11*$^{-/-}$ MCEnC early and late passages indicating the number of genes differentially expressed in the same direction in each of the sample sets. (E) Heatmap of top 30 most highly differentially expressed genes shared between *SLC4A11* KD pHCEnC, *Slc4a11*$^{-/-}$ MCEnC early and late passages. Genes are clustered based on cellular localization of the gene product.

Figure 2. Inhibition of multiple metabolic pathways in SLC4A11-deficient corneal endothelial cells. (A) Heatmap showing consensually enriched IPA canonical pathways from comparison of transcriptomes of *SLC4A11* KD pHCEnC, *Slc4a11*$^{-/-}$ MCEnC early and late passages (sorted by mean "activation z-score") (B) Schematic illustration of the crosstalk between identified inhibited metabolic pathways. Differentially expressed genes encoding key enzymes are color coded using the same color as used in C-I. Transcript levels of differentially expressed enzyme-coding genes involved in: (C) citric acid (TCA) cycle (*IDH3G,* isocitrate dehydrogenase 3 (NAD^+) gamma; *SUCLA2,* succinate-CoA ligase ADP-forming beta subunit; *SDHD,* succinate dehydrogenase complex subunit D; and *FH,* fumarate hydratas); (D) glycolysis (*GLUT1/3,* glucose transporter type 1 and 3; *GPI,* glucose-6-phosphate isomerase; *PFKL,* phosphofructokinase, liver type; *PFKP,* phosphofructokinase, platelet; *ALDOA,* aldolase, fructose-bisphosphate A; *TPI1,* triosephosphate isomerase 1; *PGK1,* phosphoglycerate kinase 1; *ENO1,* enolase 1; and *LDHD,* lactate dehydrogenase); (E) acetyl-CoA biosynthesis/pyruvate dehydrogenase (PDH) complex (*PDK3*, pyruvate dehydrogenase kinase 3; *PDHB*, pyruvate dehydrogenase E1 beta subunit; and *DLAT*, dihydrolipoamide S-acetyltransferase); (F) glutaminolysis (*SNAT1*, system N amino acid transporter 1; and *GOT2*, glutamic-oxaloacetic transaminase 2); (G) pentose phosphate shunt (*G6PD*, glucose-6-phosphate dehydrogenase; and *PGD*, phosphogluconate dehydrogenase); (H) GDP-Mannose synthesis (*MPI*, mannose phosphate isomerase; *GMPPB*, GDP-mannose pyrophosphorylase B in UDP-acetyl-galactosamine synthesis; *GNPDA1*, glucosamine-6-phosphate deaminase 1; and *PGM2L1*, phosphoglucomutase 2 like 1); (I) pyrimidine ribonucleotides (UTP/CTP) and pyrimidine deoxyribonucleotides (dTTP/dCTP) *de novo* synthesis (*CAD*, carbamoyl-

phosphate synthetase 2, aspartate transcarbamylase, and dihydroorotase; *CMPK1*, cytidine/uridine monophosphate kinase 1; *RRM1*, ribonucleotide reductase catalytic subunit M1; *RRM2*, ribonucleotide reductase regulatory subunit M2; *NME1*, NME/NM23 nucleoside diphosphate kinase 1 and *NME2*, NME/NM23 nucleoside diphosphate kinase 2). (J) Selected differentially expressed genes from each pathway listed above were validated by qPCR in separate RNA isolations from *SLC4A11* KD pHCEnC and *Slc4a11*$^{-/-}$ MCEnC early and late passages. Genes from different pathways are clustered and separated by dashed lines.

Figure 3. SLC4A11 deficiency impacts corneal endothelial ion and solute transport *function*. (A) Heatmap showing consensually enriched IPA biological function pathways from comparison of transcriptomes of SLC4A11 KD pHCEnC, Slc4a11$^{-/-}$ MCEnC early and late passages (sorted by mean "activation z-score"). (B) Representative trace of current-clamped single cell recording during 10 mM NH_4Cl superfusion of *Slc4a11*$^{+/+}$ and *Slc4a11*$^{-/-}$ MCEnC. (C) Boxplot of membrane potential changes (*d* Vm) in *Slc4a11*$^{+/+}$ (n = 6) and *Slc4a11*$^{-/-}$ (n =7) MCEnC in response to NH_4Cl superfusion. Each individual data point is plotted as a dot. [Monte Carlo resampling two-tailed paired-sampled t-test, difference between genotype *Δ*Vm = -22.2 (-34.8, -10) mV*, p* = 0.0069]. (D) Heatmap showing common differentially expressed genes encoding ion channel and transporter proteins in *SLC4A11* KD pHCEnC and early and late *Slc4a11*$^{-/-}$ MCEnC. (E) The differential expression of Na^+-HCO_3^- transporter (NBCe1, encoded by *SLC4A4*) mRNA was validated by qPCR in separate RNA isolations from *SLC4A11* KD pHCEnC and *Slc4a11*$^{-/-}$ MCEnC. (F) Western Blot for NBCe1 in *SLC4A11* KD pHCEnC and scRNA pHCEnC control showing decreased NBCe1 protein level in *SLC4A11* KD pHCEnC. (G) Representative images of immunofluorescence staining for NBCe1 (green signal) and tight junction ZO-1 (red signal) in corneal endothelium of two individuals with CHED and healthy control. Nuclei were stained with DAPI (blue signal) (scale bar, 10 μm). (H) Scatterplot of mean fluorescence intensity (MFI) ratio of NBCe1 over ZO-1 in corneal endothelium of two individuals with CHED and of seven healthy controls. (two-tailed unpaired t-test with Welch's correction, *p* = 0.0031). (I) Representative trace of intracellular pH (pH_i) response in *Slc4a11*$^{-/-}$ and *Slc4a11*$^{+/+}$ MCEnC to addition of extracellular Na^+ in HCO_3^- containing solution. (J) Bar graph of the rate of

intracellular [H^+] change (d[H^+]/ds) in *Slc4a11*$^{+/+}$ (n = 6) and *Slc4a11*$^{-/-}$ (n =8) MCEnC (two tailed unpaired t-test, $p < 0.0001$).

Figure 4. Mitochondria dysfunction in SLC4A11 deficient corneal endothelium. (A) Heatmap of commonly enriched IPA canonical and biological function pathways in transcriptomes of *SLC4A11* KD pHCEnC, early and late Slc4a11$^{-/-}$ MCEnC without assigned activation z-scores (sorted by mean "adjusted p-value"). (B) Transcript levels of differentially expressed enzyme coding genes involved in mitochondria electron transport chain (Complex I: *NDUFA1, NDUFA9, NDUFA10*, NADH:Ubiquinone Oxidoreductase subunit A1, 9 and 10; *NDUFAB1,* NADH:Ubiquinone Oxidoreductase Subunit AB1; Complex II: SDHD, Succinate Dehydrogenase Complex Subunit D; Complex III: *UQCRB*, Ubiquinol-Cytochrome C Reductase Binding Protein; *UQCRC2*, Ubiquinol-Cytochrome C Reductase Core Protein 2; *CYC1*, Cytochrome C1; Complex IV: *COX5A*, COX5B and *COX7B*, Cytochrome C Oxidase Subunit 5A, 5B and 7B; Complex V: *ATP5F1*, ATP Synthase Peripheral Stalk-Membrane Subunit B; *ATP5G1*, ATP Synthase Membrane Subunit C Locus 1). (C) Transcript levels of differentially expressed protein coding genes that serve as mitochondrial functional markers (ATP flux: *VDAC2/3,* Voltage-dependent Anion-selective Channel; import machinery: *TIMM7A, TIMM8A, TIMM50*, Translocase of Inner Mitochondrial Membrane 7A, 8A, 50; translation machinery: *GFM2,* G Elongation Factor Mitochondrial 2*; MRPL10, MRPL18, MRPL20, MRPL33, MRPL48, MRPL52, MRPL58, MRPL16, MRPS2, MRPS18A,* Mitochondrial Ribosomal Protein L10*,* L18, L20, L33, L48, L52, L58, L16, S2, S18A;). (D) Transcript levels of differentially expressed *STX17* in *SLC4A11* KD pHCEnC and *Slc4a11*$^{-/-}$ MCEnC transcriptomes. (E) Differential expression of *STX17* mRNA in *SLC4A11* KD pHCEnC and *Slc4a11*$^{-/-}$ MCEnC validated by qPCR in separate RNA isolations. (F) Western Blot for STX17 and NBCe1in scRNA pHCEnC control and SLC4A11 KD pHCEnC showing decreased protein level in *SLC4A11* KD pHCEnC*.*

(G) Representative images of immunofluorescence staining for STX17 (green signal) and mitochondria marker COX4 (red signal) in corneal endothelium of two individuals with CHED and healthy control. Nuclei were stained with DAPI (blue signal)(scale bar, 10 μm). (H) Scatterplot of mean fluorescence intensity (MFI) ratio of STX17 over COX4 in corneal endothelium of two individuals with CHED and of seven healthy controls (two-tailed unpaired t-test with Welch's correction, $p = 0.0483$). (I) Scatterplot of MFI of COX4 in corneal endothelium of two individuals with CHED and of seven healthy controls (two-tailed unpaired t-test with Welch's correction, $p = 0.0018$). (J) Representative images of immunofluorescence staining for cytochrome C (green signal) in corneal endothelium of two individuals with CHED and of seven healthy controls. Nucleus were stained with DAPI (blue signal) (scale bar, 5 μm). (K) Scatterplot of MFI of cytochrome C in corneal endothelium of two individuals with CHED and of seven healthy controls (two-tailed unpaired t-test with Welch's correction, $p = 0.0304$). (L) Bar graph summary of intracellar ATP levels measured in *SLC4A11* KD pHCEnC and scRNA pHCEnC controls (n = 6 each, one-tailed unpaired t-test, $p = 0.0281$). (M) Bar graph summary of intracellar ATP levels measured in early passage (n=6 each, two-tailed unpaired t-test, $p = 0.034$) and late passage (n=6 each, $p = 0.039$) *Slc4a11*$^{+/+}$ and *Slc4a11*$^{-/-}$ MCEnC.

Figure 5. Activation of AMPK-p53 pathway in SLC4A11 deficient corneal endothelium. (A) Heatmap of shared predicted upstream regulators of transcriptomes of SLC4A11 KD pHCEnC, early and late Slc4a11$^{-/-}$ MCEnC (sorted by mean "adjusted p-value"). (B) Western blot analysis of *SLC4A11* KD pHCEnC and scRNA controls for SLC4A11, Ser15 phosphorylated p53 (phos-p53 (S15)), total p53, Thr172 phosphorylated AMPKα (phos-AMPKα (T172)), total AMPKα, Ser182 phosphorylated AMPKβ (phos-AMPKβ1 (S182)) and total AMPKβ1 and β2. (C) Western blot analysis of early and late *Slc4a11*$^{+/+}$ and *Slc4a11*$^{-/-}$ MCEnC for Ser18 phosphorylated p53 (phos-p53 (S18)), total p53, Thr172 phosphorylated AMPKα (phos-AMPKα (T172)), total AMPKα, Ser182 phosphorylated AMPKβ (phos-AMPKβ1 (S182)) and total AMPKβ1 and β2. (D) Bar graph summary of Western blot densitometry results for normalized total p53 level in *SLC4A11* KD pHCEnC versus scRNA pHCEnC (CTRL) (two-tailed unpaired-sample t-test, $p > 0.99$), in early passage *Slc4a11*$^{-/-}$ versus *Slc4a11*$^{+/+}$ MCEnC ($p = 0.00027$) and late passage *Slc4a11*$^{-/-}$ versus *Slc4a11*$^{+/+}$ MCEnC ($p = 0.00027$).

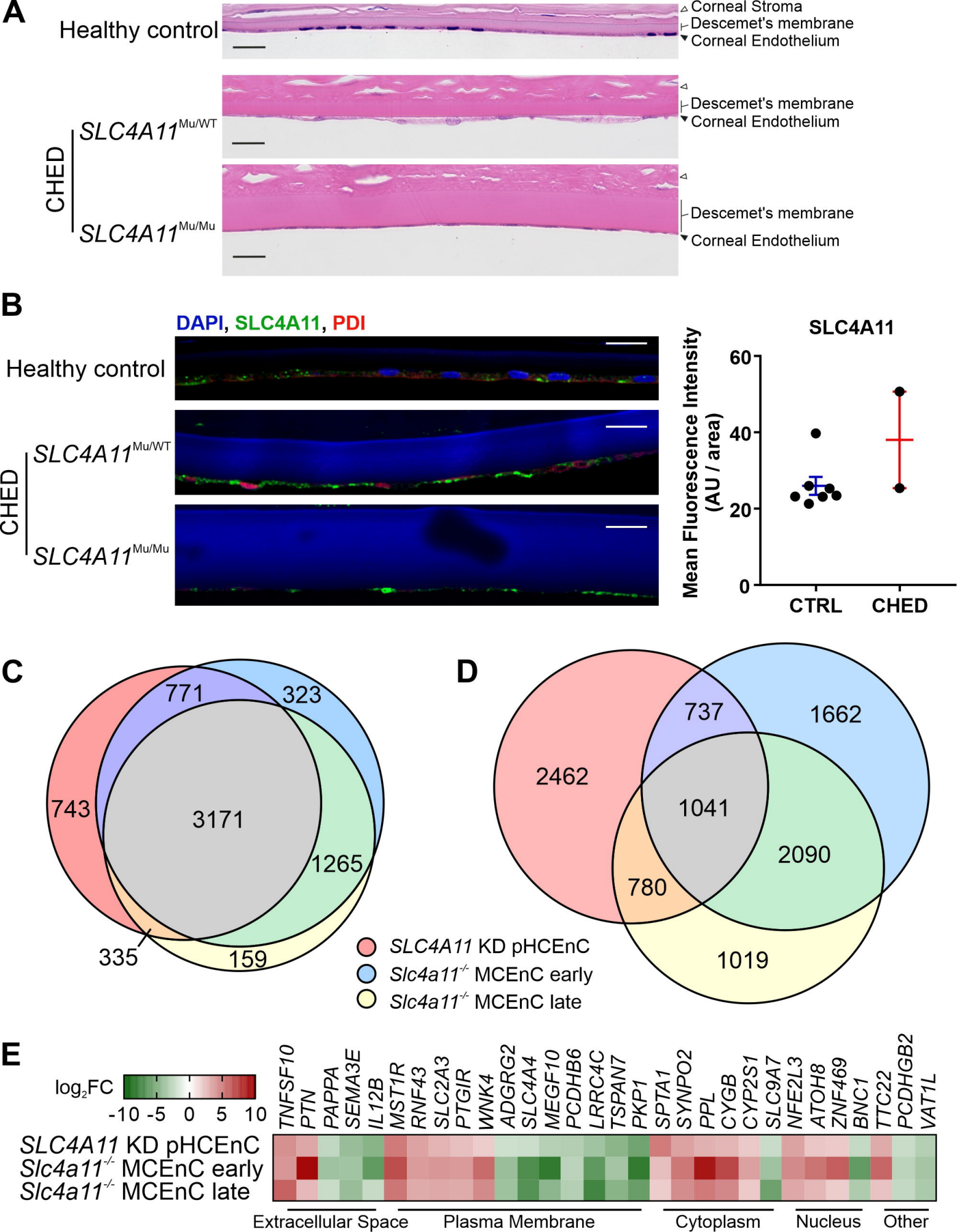
A
Healthy control
Corneal Stroma
Descemet's membrane
Corneal Endothelium
CHED
SLC4A11Mu/WT
SLC4A11Mu/Mu
B
DAPI, SLC4A11, PDI
SLC4A11
Mean Fluorescence Intensity (AU / area)
CTRL
C
771
323
743
3171
1265
335
159
D
737
1662
2462
1041
2090
780
1019
SLC4A11 KD pHCEnC
Slc4a11-/- MCEnC early
Slc4a11-/- MCEnC late
E
log2FC
-10 -5 0 5 10
TNFSF10 PTN PAPPA SEMA3E IL12B MST1R RNF43 SLC2A3 PTGIR WNK4 ADGRG2 SLC4A4 MEGF10 PCDHB6 LRRC4C TSPAN7 PKP1 SPTA1 SYNPO2 PPL CYGB CYP2S1 SLC9A7 NFE2L3 ATOH8 ZNF469 BNC1 TTC22 PCDHGB2 VAT1L
Extracellular Space
Plasma Membrane
Cytoplasm
Nucleus
Other

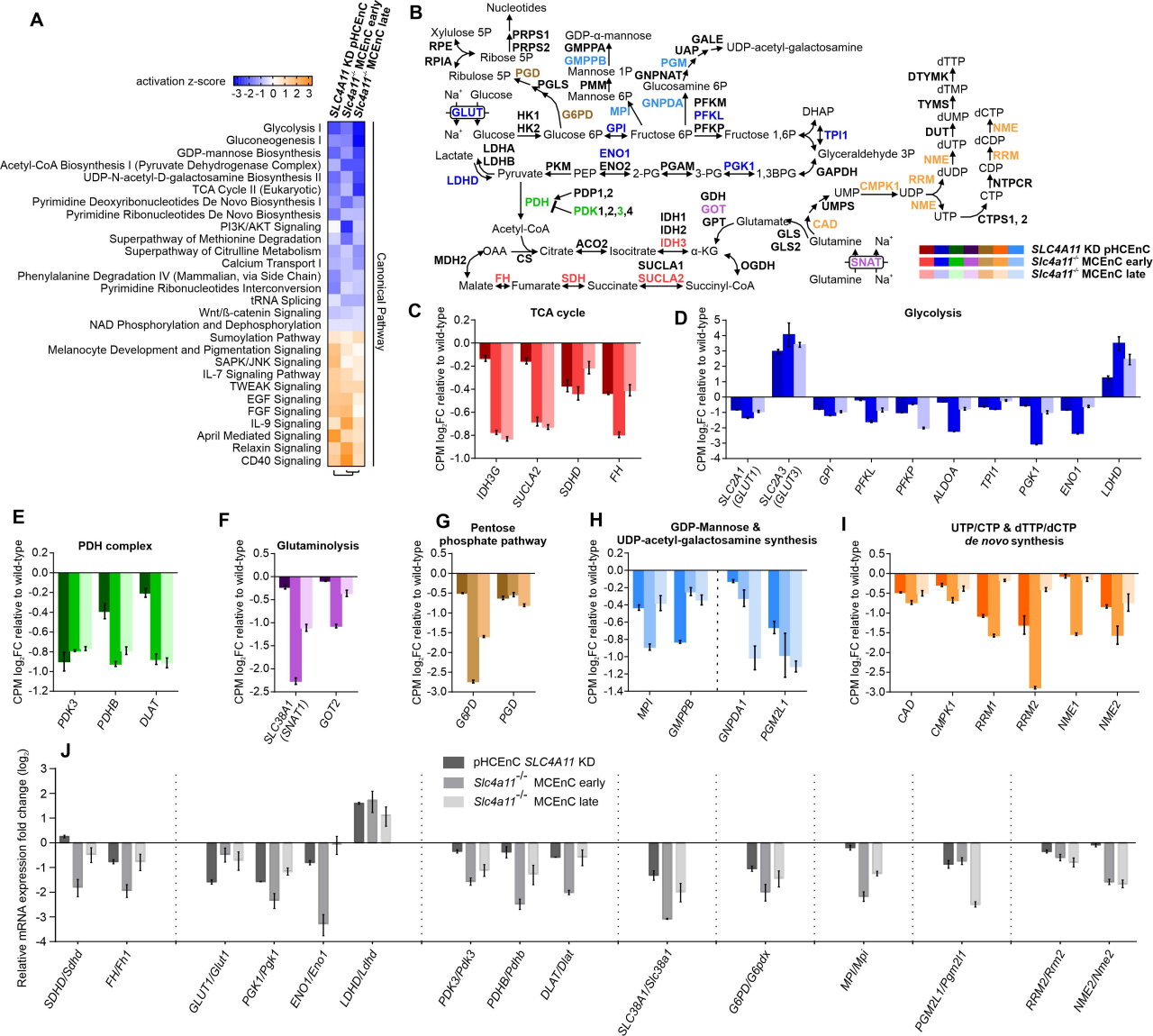
A
activation z-score
-3 -2 -1 0 1 2 3
SLC4A11 KD pHCEnC
Slc4a11-/- MCEnC early
Slc4a11-/- MCEnC late
Glycolysis I
Gluconeogenesis I
GDP-mannose Biosynthesis
Acetyl-CoA Biosynthesis I (Pyruvate Dehydrogenase Complex)
UDP-N-acetyl-D-galactosamine Biosynthesis II
TCA Cycle II (Eukaryotic)
Pyrimidine Deoxyribonucleotides De Novo Biosynthesis I
Pyrimidine Ribonucleotides De Novo Biosynthesis
PI3K/AKT Signaling
Superpathway of Methionine Degradation
Superpathway of Citrulline Metabolism
Calcium Transport I
Phenylalanine Degradation IV (Mammalian, via Side Chain)
Pyrimidine Ribonucleotides Interconversion
tRNA Splicing
Wnt/ß-catenin Signaling
NAD Phosphorylation and Dephosphorylation
Sumoylation Pathway
Melanocyte Development and Pigmentation Signaling
SAPK/JNK Signaling
IL-7 Signaling Pathway
TWEAK Signaling
EGF Signaling
FGF Signaling
IL-9 Signaling
April Mediated Signaling
Relaxin Signaling
CD40 Signaling
Canonical Pathway
B
Nucleotides
Xylulose 5P
RPE
RPIA
Ribose 5P
PRPS1
PRPS2
GDP-α-mannose
GMPPA
GMPPB
Mannose 1P
GALE
UAP
UDP-acetyl-galactosamine
PGM
GNPNAT
Glucosamine 6P
Ribulose 5P
PGD
PGLS
PMM
Mannose 6P
Na+ Glucose
GLUT
HK1
HK2
G6PD
MPI
GNPDA
PFKM
PFKL
PFKP
Na+ Glucose
Glucose 6P
GPI
Fructose 6P
Fructose 1,6P
DHAP
TPI1
Glyceraldehyde 3P
GAPDH
Lactate
LDHA
LDHB
LDHD
Pyruvate
PKM
PEP
ENO1
ENO2
2-PG
PGAM
3-PG
PGK1
1,3BPG
PDH
PDP1,2
PDK1,2,3,4
Acetyl-CoA
OAA
CS
Citrate
ACO2
Isocitrate
IDH1
IDH2
IDH3
α-KG
GDH
GOT
GPT
Glutamate
GLS
GLS2
Glutamine
Na+
SNAT
Glutamine
Na+
MDH2
Malate
FH
Fumarate
SDH
Succinate
SUCLA1
SUCLA2
Succinyl-CoA
OGDH
dTTP
DTYMK
dTMP
TYMS
dUMP
DUT
dUTP
NME
dUDP
RRM
UMP
CMPK1
UDP
NME
UTP
CTP
CTPS1, 2
dCTP
NME
dCDP
RRM
CDP
NTPCR
SLC4A11 KD pHCEnC
Slc4a11-/- MCEnC early
Slc4a11-/- MCEnC late
C
TCA cycle
CPM log2FC relative to wild-type
IDH3G
SUCLA2
SDHD
FH
D
Glycolysis
CPM log2FC relative to wild-type
SLC2A1 (GLUT1)
SLC2A3 (GLUT3)
GPI
PFKL
PFKP
ALDOA
TPI1
PGK1
ENO1
LDHD
E
PDH complex
CPM log2FC relative to wild-type
PDK3
PDHB
DLAT
F
Glutaminolysis
CPM log2FC relative to wild-type
SLC38A1 (SNAT1)
GOT2
G
Pentose phosphate pathway
CPM log2FC relative to wild-type
G6PD
PGD
H
GDP-Mannose & UDP-acetyl-galactosamine synthesis
CPM log2FC relative to wild-type
MPI
GMPPB
GNPDA1
PGM2L1
I
UTP/CTP & dTTP/dCTP de novo synthesis
CPM log2FC relative to wild-type
CAD
CMPK1
RRM1
RRM2
NME1
NME2
J
pHCEnC SLC4A11 KD
Slc4a11-/- MCEnC early
Slc4a11-/- MCEnC late
Relative mRNA expression fold change (log2)
SDHD/Sdhd
FH/Fh1
GLUT1/Glut1
PGK1/Pgk1
ENO1/Eno1
LDHD/Ldhd
PDK3/Pdk3
PDHB/Pdhb
DLAT/Dlat
SLC38A1/Slc38a1
G6PD/G6pdx
MPI/Mpi
PGM2L1/Pgm2l1
RRM2/Rrm2
NME2/Nme2

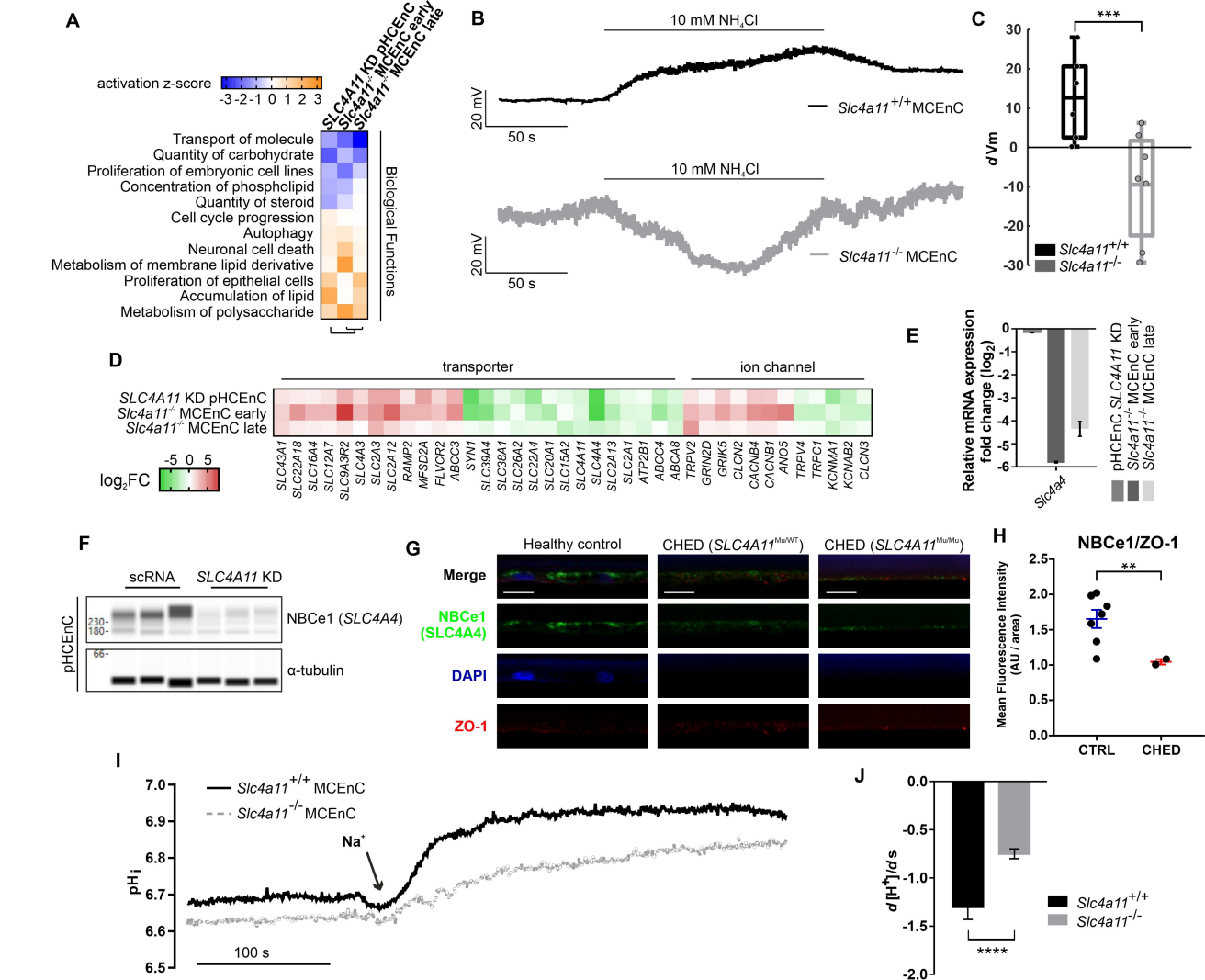
A
activation z-score
-3 -2 -1 0 1 2 3
SLC4A11 KD pHCEnC
Slc4a11-/- MCEnC early
Slc4a11-/- MCEnC late
Transport of molecule
Quantity of carbohydrate
Proliferation of embryonic cell lines
Concentration of phospholipid
Quantity of steroid
Cell cycle progression
Autophagy
Neuronal cell death
Metabolism of membrane lipid derivative
Proliferation of epithelial cells
Accumulation of lipid
Metabolism of polysaccharide
Biological Functions
B
10 mM NH4Cl
20 mV
50 s
Slc4a11+/+ MCEnC
10 mM NH4Cl
20 mV
50 s
Slc4a11-/- MCEnC
C
***
dVm
Slc4a11+/+
Slc4a11-/-
D
transporter
ion channel
SLC4A11 KD pHCEnC
Slc4a11-/- MCEnC early
Slc4a11-/- MCEnC late
log2FC
-5 0 5
SLC43A1
SLC22A18
SLC16A4
SLC12A7
SLC9A3R2
SLC4A3
SLC2A3
SLC2A12
RAMP2
MFSD2A
FLVCR2
ABCC3
SYN1
SLC39A4
SLC38A1
SLC26A2
SLC22A4
SLC20A1
SLC15A2
SLC4A11
SLC4A4
SLC2A13
SLC2A1
ATP2B1
ABCC4
ABCA8
TRPV2
GRIN2D
GRIK5
CLCN2
CACNB4
CACNB1
ANO5
TRPV4
TRPC1
KCNMA1
KCNAB2
CLCN3
E
Relative mRNA expression fold change (log2)
Slc4a4
pHCEnC SLC4A11 KD
Slc4a11-/- MCEnC early
Slc4a11-/- MCEnC late
F
scRNA
SLC4A11 KD
pHCEnC
230-
180-
NBCe1 (SLC4A4)
66-
α-tubulin
G
Healthy control
CHED (SLC4A11Mu/WT)
CHED (SLC4A11Mu/Mu)
Merge
NBCe1 (SLC4A4)
DAPI
ZO-1
H
NBCe1/ZO-1
**
Mean Fluorescence Intensity (AU / area)
CTRL
CHED
I
Slc4a11+/+ MCEnC
Slc4a11-/- MCEnC
Na+
pHi
100 s
J
d[H+]/ds
Slc4a11+/+
Slc4a11-/-
****

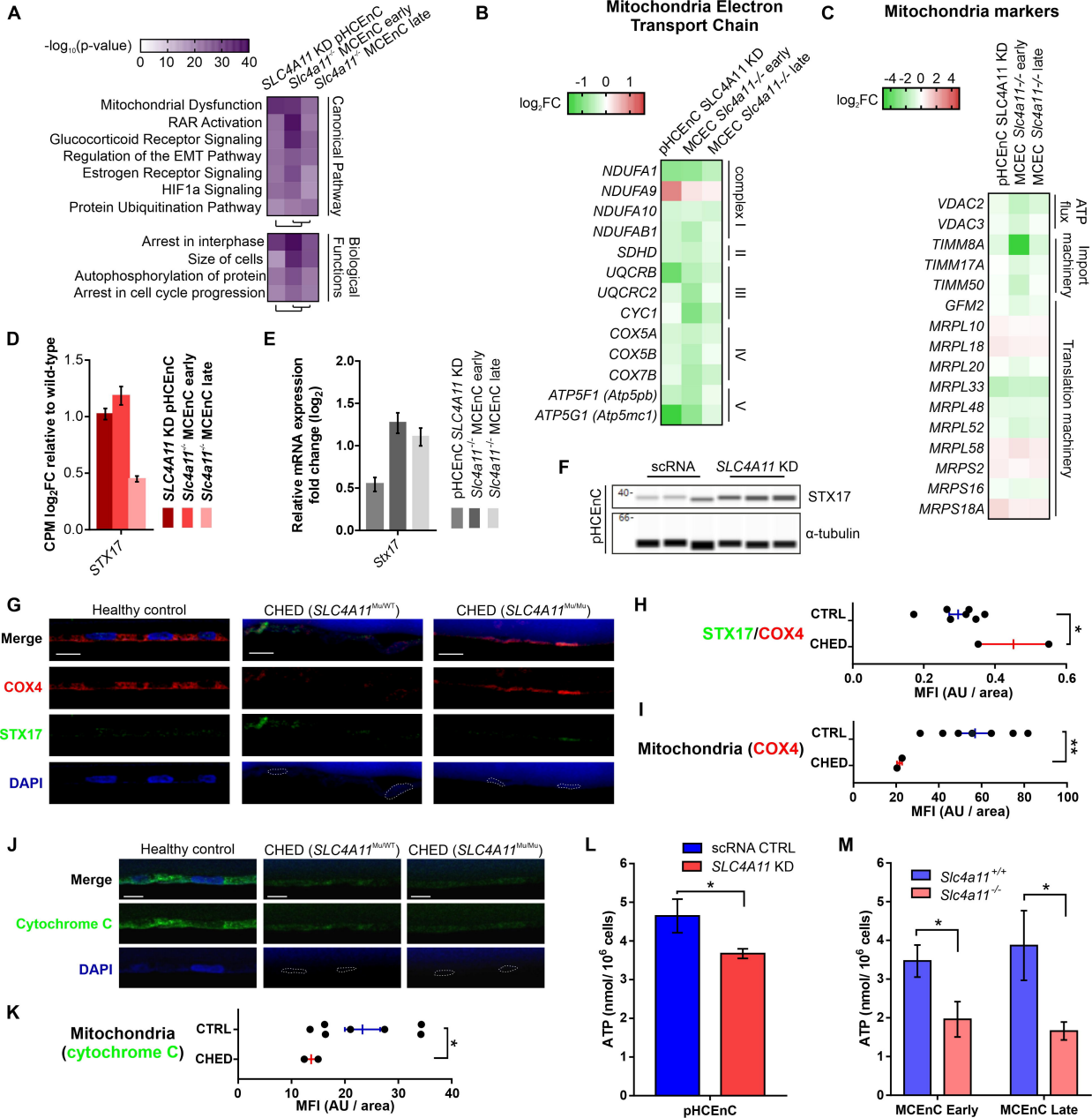
A
-log10(p-value)
0 10 20 30 40
SLC4A11 KD pHCEnC
Slc4a11-/- MCEnC early
Slc4a11-/- MCEnC late
Mitochondrial Dysfunction
RAR Activation
Glucocorticoid Receptor Signaling
Regulation of the EMT Pathway
Estrogen Receptor Signaling
HIF1a Signaling
Protein Ubiquitination Pathway
Canonical Pathway
Arrest in interphase
Size of cells
Autophosphorylation of protein
Arrest in cell cycle progression
Biological Functions
B
Mitochondria Electron Transport Chain
log2FC
-1 0 1
pHCEnC SLC4A11 KD
MCEC Slc4a11-/- early
MCEC Slc4a11-/- late
NDUFA1
NDUFA9
NDUFA10
NDUFAB1
SDHD
UQCRB
UQCRC2
CYC1
COX5A
COX5B
COX7B
ATP5F1 (Atp5pb)
ATP5G1 (Atp5mc1)
complex I
II
III
IV
V
C
Mitochondria markers
log2FC
-4 -2 0 2 4
pHCEnC SLC4A11 KD
MCEC Slc4a11-/- early
MCEC Slc4a11-/- late
VDAC2
VDAC3
TIMM8A
TIMM17A
TIMM50
GFM2
MRPL10
MRPL18
MRPL20
MRPL33
MRPL48
MRPL52
MRPL58
MRPS2
MRPS16
MRPS18A
ATP flux
Import machinery
Translation machinery
D
CPM log2FC relative to wild-type
1.5
1.0
0.5
0.0
STX17
SLC4A11 KD pHCEnC
Slc4a11-/- MCEnC early
Slc4a11-/- MCEnC late
E
Relative mRNA expression fold change (log2)
2.0
1.5
1.0
0.5
0.0
Stx17
pHCEnC SLC4A11 KD
Slc4a11-/- MCEnC early
Slc4a11-/- MCEnC late
F
scRNA
SLC4A11 KD
pHCEnC
40-
66-
STX17
α-tubulin
G
Healthy control
CHED (SLC4A11Mu/WT)
CHED (SLC4A11Mu/Mu)
Merge
COX4
STX17
DAPI
H
STX17/COX4
CTRL
CHED
*
0.0 0.2 0.4 0.6
MFI (AU / area)
I
Mitochondria (COX4)
CTRL
CHED
**
0 20 40 60 80 100
MFI (AU / area)
J
Healthy control
CHED (SLC4A11Mu/WT)
CHED (SLC4A11Mu/Mu)
Merge
Cytochrome C
DAPI
K
Mitochondria (cytochrome C)
CTRL
CHED
*
0 10 20 30 40
MFI (AU / area)
L
scRNA CTRL
SLC4A11 KD
ATP (nmol/ 10^6 cells)
*
pHCEnC
M
Slc4a11+/+
Slc4a11-/-
ATP (nmol/ 10^6 cells)
*
*
MCEnC Early
MCEnC Late

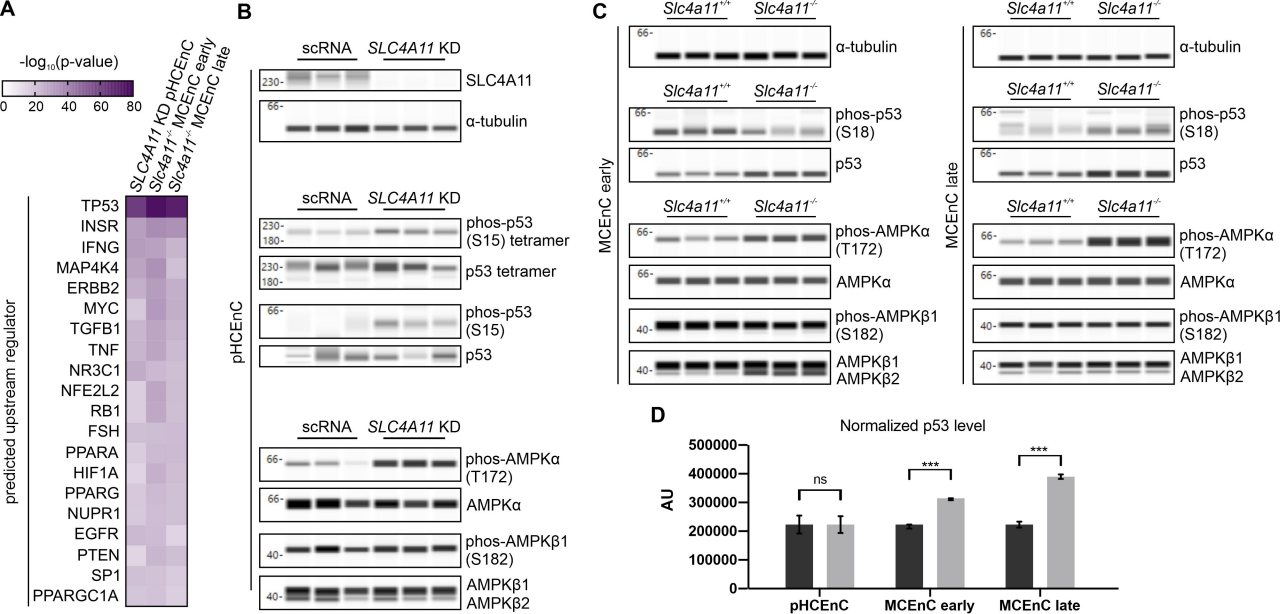
A
-log10(p-value)
0
20
40
60
80
SLC4A11 KD pHCEnC
Slc4a11-/- MCEnC early
Slc4a11-/- MCEnC late
predicted upstream regulator
TP53
INSR
IFNG
MAP4K4
ERBB2
MYC
TGFB1
TNF
NR3C1
NFE2L2
RB1
FSH
PPARA
HIF1A
PPARG
NUPR1
EGFR
PTEN
SP1
PPARGC1A
B
pHCEnC
scRNA
SLC4A11 KD
SLC4A11
α-tubulin
phos-p53 (S15) tetramer
p53 tetramer
phos-p53 (S15)
p53
phos-AMPKα (T172)
AMPKα
phos-AMPKβ1 (S182)
AMPKβ1
AMPKβ2
C
MCEnC early
MCEnC late
Slc4a11+/+
Slc4a11-/-
phos-p53 (S18)
D
Normalized p53 level
AU
500000
400000
300000
200000
100000
0
ns
***
pHCEnC
MCEnC early
MCEnC late